Available online at www.sciencedirect.com
ScienceDirect
Journal of Solid State Chemistry 181 (2008) 457–466
JOURNAL OF SOLID STATE CHEMISTRY
www.elsevier.com/locate/jssc

2D parallel interpenetration of $[M_2(bpp)_4X_4]$ [*M*, Fe(II)/Co(II); bpp, 4,4′-trimethylenedipyridine; *X*, SCN^-, $SeCN^-$ and N_3^-] complexes: Pseudohalide-dependent conformation of bpp

Subal Chandra Manna[a], Atish Dipankar Jana[b], Georgina M. Rosair[c], Michael G.B. Drew[d], Golam Mostafa[b,*], Nirmalendu Ray Chaudhuri[a]

[a]*Department of Inorganic Chemistry, Indian Association for the Cultivation of Science, Kolkata 700032, India*
[b]*Department of Physics, Jadavpur University, Kolkata 700032, India*
[c]*Department of Chemistry, School of Engineering and Physical Sciences, Heriot-Watt University, Riccarton, Edinburgh EH14 4AS, UK*
[d]*Department of Chemistry, The University of Reading, Whiteknights, Reading RG6 6AD, UK*

Received 27 August 2007; received in revised form 2 December 2007; accepted 9 December 2007
Available online 23 December 2007

Abstract

Three coordination complexes of Co(II)/Fe(II) with 4,4′-trimethylenedipyridine (bpp) and pseudohalides (SCN^-, $SeCN^-$ and N_3^-) have been synthesized. The complexes have been characterized by X-ray single crystal structure determination. They are isomorphous having 2D layers in which two independent wavy nets display parallel interwoven structures. Pseudohalide binds metal centers through N terminal and occupies the *trans* axial positions of the octahedral metal coordination environment. Pseudohalide remains pendant on both sides of the polymeric layer and help the stacking through hydrogen bonding. The conformation of bpp in the interpenetrated nets is observed to be dependent on the choice of pseudohalide.

Keywords: 4, 4′-trimethylenedipyridine; Fe(II); Co(II); Pseudohalide; Interpenetration; Supramolecule

1. Introduction

Self-assembled extended metal-organic frameworks (MOF) as functional materials with specific network topologies are of great interest due to their fascinating architectures [1–8] and potential applications in the field of magnetism [9], electrical conductivity [10], ion exchange [11], separation [12,13], biology [14] and catalysis [15–18]. The nature of the bridging ligand is of utmost importance considering that it actively determines the topology of the coordination polymers and also its functionality. Flexible building blocks with a number of conformational degrees of freedom often efficiently participate in the self-assembly process adopting suitable conformation that stabilizes the assembly in an optimal manner. Long spacers (rigid/flexible) have been used [19,20] in the quest of porous materials, but they generally yield interpenetrated networks with reduced/no void space, with a few exceptions where substantial amount of void space persists even after interpenetration [21]. The appearance of interpenetration is due to the natural tendency of molecular building blocks to pack most efficiently in the crystalline state. A large variety of interpenetrating [22–31] structures have been determined, but the simplest among them is the parallel interpenetration of two nets [32]. The long 4,4′-trimethylenedipyridine (bpp) has often been used for construction of MOF, but due to its flexibility with various conformational degrees of freedom (TG, TT, GG′, GG) [33] (Scheme 1), it often results interpenetrated networks with various network topologies. Both 3D interpenetration with dimondiod network and 2D interpenetration with (4,4) net topology have been observed with bpp. The metal–metal separation

*Corresponding authors. Fax: +91 33 2473 2805.
E-mail addresses: mostafa_ju@yahoo.co.in (G. Mostafa), icnrc@iacs.res.in (N. Ray Chaudhuri).

0022-4596/$ - see front matter © 2008 Elsevier Inc. All rights reserved.
doi:10.1016/j.jssc.2007.12.009

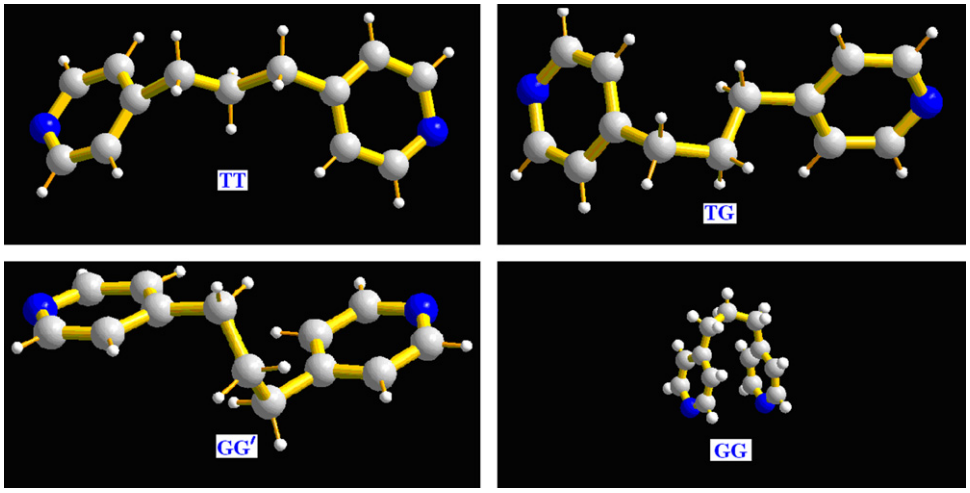

Scheme 1.

on the network depends on the conformational choice of bpp in these networks. In the TT mode bpp separates two consecutive metal centers the farthest and in GG mode the least. Any crystal engineering effort using bpp as one of the ligands thus needs a clear understanding about the factors on which the conformation of bpp depends. A suitable strategy for designing (4,4) net architecture is to use bidentate linear spacer and transition metal that has preference for octahedral coordination geometry with linear pseudohalide as coligand that can possibly bind the axial sites. Using this strategy recently our group has reported $[Fe_2(bpp)_4(N_3)_4]$ [34], $[Mn_2(bpp)_4(OCN)_4]$ [35]; both of them possess parallel interpenetrated 2D structure and in the present contribution we wish to report three new complexes $[Fe(bpp)_2(NCS)_2]$ (**1**), $[Co_2(bpp)_4(SeCN)_4]$ (**2**) and $[Co_2(bpp)_4(N_3)_4]$ (**3**) all having 2D interpenetrated networks. There are limited number of transition metal–bpp complexes [34–37] in combination with the pseudohalide (N_3^-, OCN^- , SCN^-, $SeCN^-$, etc.). So a careful analysis of the reported structures along with the present complexes has been carried out to understand the conformational preferences of bpp in this class of complexes, which indicates that besides transition metals, associated pseudohalides also play important role.

2. Experimental section

2.1. Materials

High purity bpp, potassium selenocyanate and sodium azide were purchased from the Aldrich Chemical Co. Inc. and were used. All other chemicals were of AR grade.

2.2. Physical measurements

Elemental analyses (carbon, hydrogen and nitrogen) were performed using a Perkin-Elmer 240C elemental analyzer. IR spectra were measured from KBr pellets on a Nicolet 520 FTIR spectrometer.

2.3. Synthesis

2.3.1. $[Fe(bpp)_2(NCS)_2]$ (**1**)

An aqueous solution (5 mL) of ammonia thiocyanate (2 mmol, 0.152 g) was added dropwise to a freshly prepared aqueous solution (5 mL) of ferrous ammonium sulfate hexahydrate (1 mol, 0.393 g) under stirring condition. To the resulting reaction mixture a methanolic solution (10 mL) of bpp (1 mmol, 0.198 g) was added and stirred for 1 h. Resulting reddish brown solution was filtered and the filtrate was kept in a $CaCl_2$ desiccator and after a week suitable black single crystals for X-ray structure determination were obtained. They were separated and washed with ethanol, and dried. Yield: 78% (0.443 g). Anal. data found: C, 58.26; H, 4.77; N, 14.45(%). Calcd. for $C_{28}H_{28}FeN_6S_2$: C, 59.10; H, 4.92; N, 14.77(%). The infrared spectra exhibited the following absorptions: 3058(w), 2952(s), 2872(w), 2049(vs), 1613(s), 1560(w), 1507(w), 1422(s), 1223(w), 1015(w), 808(w), 565(vw), 512(w) cm^{-1}.

2.3.2. $[Co_2(bpp)_4(SeCN)_4]$ (**2**)

An aqueous solution (15 mL) of potassium selenocyanate (2 mmol; 0.288 g) was added dropwise to a methanolic solution (5 mL) of cobalt nitrate hexahydrate (1 mmol; 0.291 g) with constant stirring. To the resulting light pink colored reaction mixture, a methanolic solution (10 mL) of bpp (1 mmol; 0.198 g) was added and stirred for 1 h. A dark brown colored complex was separated out. The single crystals suitable for X-ray analysis were obtained by diffusing the methanolic solution (10 mL) of bpp on an aqueous layer of $Co(NO_3)_2 \cdot 6H_2O$ and potassium selenocyanate (1:2 mixture) (10 mL) in a tube. The reddish brown crystals suitable for X-ray analysis were deposited at the junction of two solutions after a few days. Yield: 70% (0.465 g). Anal. data found: C, 49.78; H, 4.11; N, 12.34(%). Calcd. for $C_{56}H_{56}Co_2N_{12}Se_4$: C, 50.49; H, 4.20; N, 12.63 (%). The infrared spectra exhibited the following absorptions: 3071(vw), 2939(s), 2059(vs), 1614(s), 1566(vw),

1507(w), 1423(s), 1223(w), 1076(vw), 1018(w), 809(w), 572(vw), 512(w) cm^{-1}.

2.3.3. $[Co_2(bpp)_4(N_3)_4]$ (3)

It was synthesized following the procedure as adopted for **2** using sodium azide (2 mmol; 0.130) instead of potassium selenocyanate. The single crystals suitable for X-ray analysis were obtained by diffusing the methanolic solution (10 mL) of bpp on an aqueous layer of $Co(NO_3)_2 \cdot 6H_2O$ and sodium azide (1:2 mixture) (10 mL) in a tube. The deep brown crystals were deposited at the junction of two solutions after a few days. Yield: 75% (0.404 g). Anal. data found: C, 56.87; H, 5.06; N, 25.51(%). Calcd. for $C_{52}H_{56}Co_2N_{20}$: C, 57.83; H, 5.19; N, 25.94(%). The infrared spectra exhibited the following absorptions: 3363(w), 2937(s), 2036(vs), 1612(s), 1556(w), 1500(w), 1421(s), 1336(w), 1220(s), 1068(vw), 1014w), 813(w), 518(w) cm^{-1}.

2.4. Crystallographic data collection and refinement

Single crystals were mounted on Mercury CCD, Bruker Smart CCD and Mar-research IP diffractometer for complexes **1**, **2** and **3**, respectively, and equipped with a graphite monochromator and Mo$K\alpha$ ($\lambda = 0.71073$ Å) radiation. The structure was solved using Patterson method by using the SHELXL software package. The correct positions for the cobalt atom were deduced from an E-map. Subsequent difference Fourier synthesis and least-square refinement revealed the positions of the remaining non-hydrogen atoms. At this point, a calculation by PLATON showed that there was no missed crystallographic symmetry. Non-hydrogen atoms were refined with independent anisotropic displacement parameters. Hydrogen atoms were placed in an idealized positions and their displacement parameters were fixed to be 30% larger than those of the attached non-hydrogen atoms. All calculations were carried out using SHELXL 97 [38] SHELXS 97 [39], PLATON 99 [40], ORTEP-32 [41] and WinGX system Ver-1.64 [42]. Data collection and structure refinement parameters and crystallographic data for all complexes are given in Table 1. The selected bond lengths, as well as hydrogen bonding interactions are summarized in Tables 2 and 3.

Table 1
Crystallographic data and details of refinements for complexes **1**–**3**

Complex	**1**	**2**	**3**
Empirical formula	$C_{28}H_{28}FeN_6S_2$	$C_{56}H_{56}Co_2N_{12}Se_4$	$C_{52}H_{56}Co_2N_{20}$
M	568.54	1330.83	1079.03
Temperature (K)	296	100	293
Crystal system	Monoclinic	Triclinic	Triclinic
Space group	$P2_1/n$ (No. 14)	$P-1$ (No. 2)	$P-1$ (No. 2)
a (Å)	18.7884(4)	11.1785(15)	11.250(14)
b (Å)	16.5851(2)	15.816(2)	14.475(17)
c (Å)	20.6845(4)	18.092(3)	17.99(2)
α (deg.)	90	92.045(4)	79.353(10)
β (deg.)	114.6640(2)	103.565(4)	81.420(10)
γ (deg.)	90	110.238(4)	72.090(10)
V (Å^3)	5857.43(18)	2893.4(7)	2726(6)
Z	8	2	2
D_c (g/cm^3) mm^{-1}	1.289	1.528	1.315
μ (mm^{-1})	0.684	3.136	0.664
Reflections collected	43,750	74,905	8867
Independent reflections	13,239	13,313	8867
No. of parameters	723	667	668
GOF(S)	1.35	0.95	1.14
Data[$I > 2\sigma(I)$]	12,000	11,796	6491
R	0.0912	0.0246	0.0827
WR_2	0.2026	0.0656	0.1648
θ range (deg.)	3.1, 27.5	1.2, 27.6	1.5, 25.8
F (000)	2368	1332	1124

3. Results and discussion

3.1. Crystal structure descriptions

General features of all three complexes are identical, metal atoms are coordinated by four nitrogen atoms from four bpp in the equatorial plane of a distorted octahedral coordination environment, two axial positions are coordinated by pseudohalide (NCS^- (1), $NCSe^-$ (2) and N_3^- (3))

Table 2
Bond distances (Å) for complexes **1**, **2** and **3**

Equatorial geometry		Axial geometry	
Complex ***1***			
Fe1–N1	2.210(3)	Fe1–N5	2.131(3)
Fe1–N2_*a*	2.226(3)	Fe1–N6	2.107(3)
Fe1–N3	2.210(3)	Fe2–N11	2.111(4)
Fe1–N4_*b*	2.244(3)	Fe2–N12	2.124(4)
Fe2–N7	2.225(4)		
Fe2–N8_*c*	2.209(4)		
Fe2–N9	2.220(4)		
Fe2–N10_*d*	2.234(4)		
Complex ***2***			
Co1–N1	2.1813(15)	Co1–N5	2.1011(18)
Co1–N2	2.1668(17)	Co1–N6	2.1138(18)
Co1–N3	2.1773(15)		
Co1–N4	2.1669(16)		
Co2–N7	2.1678(18)	Co2–N11	2.1110(16)
Co2–N8	2.1819(16)	Co2–N12	2.1149(17)
Co2–N9	2.1707(18)		
Co2–N10	2.1735(15)		
Complex ***3***			
Co1–N1	2.32(5)		
Co1–N3	2.337(4)		
Co1–N2	2.351(5)	Co1–N5	2.118(5)
Co1–N4	2.329(4)	Co1–N6	2.123(5)
Co2–N7	2.313(4)		
Co2–N8_*e*	2.350(4)		
Co2–N10_*f*	2.325(4)	Co2–N11	2.140(5)
Co2–N9_*g*	2.352(5)	Co2–N12	2.117(5)

Symmetry transformations used to generate equivalent atoms: $a = 3/2-x, 1/2+y, 3/2-z$; $b = 1/2-x, -1/2+y, 3/2-z$; $c = 3/2-x, 1/2+y, 3/2-z$; $d = 1/2-x, -1/2+y, 3/2-z$; $e = x, -1+y, z$; $f = -1+x, y, 1+z$; $g = -1+x, -1+y, 1+z$.

Table 3
Hydrogen bonding interactions for the complexes **1–3**

D–H···A	D–H	H···A	D···A	<D–H···A	Symmetry
Complex ***1***					
C25–H25···N5	0.93	2.62	3.14(5)	116.00	$1/2-x$, $1/2+y$, $3/2-z$
C39—H39···S3	0.93	2.83	3.627(4)	145.00	$1-x$, $1-y$, $1-z$
Complex ***2***					
C29–H11c···N5	0.95	2.62	3.151(3)	116.00	
C45–H31c···Se2	0.95	2.94	3.513(2)	120.00	$-1+x$, $-1+y$, z
C51–H32a···Se1	0.95	2.93	3.716(2)	141.00	$1-x$, $2-y$, $1-z$
Complex ***3***					
C4–H4···N112	0.93	2.46	3.391(8)	176.00	$1+x$, y, z
C5–H5···N5	0.93	2.57	3.161(7)	122.00	
C15–H15···N62	0.93	2.58	3.429(7)	151.00	$1-x$, $2-y$, $2-z$
C26–H26···N112	0.93	2.53	3.399(7)	156.00	$1-x$, $2-y$, $2-z$
C30–H30···N52	0.93	2.55	3.403(7)	152.00	$2-x$, $2-y$, $1-z$
C40–H40···N6	0.93	2.62	3.204(7)	121.00	
C49–H49···N62	0.93	2.45	3.349(7)	163.00	$1-x$, $2-y$, $1-z$
C50–H50···N11	0.93	2.54	3.153(7)	124.00	$1+x$, y, $-1+z$

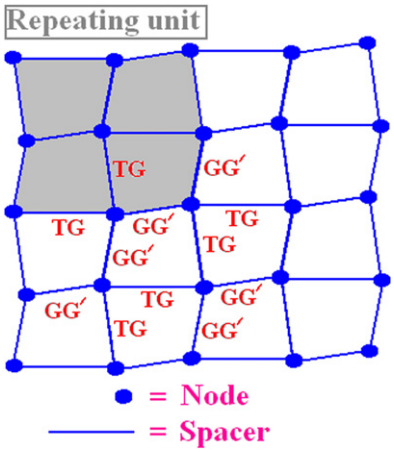

Scheme 2.

through N atoms. The bpp functions as bridging ligand to produce undulated 2D network with (4,4) net topology. Two crystallographically independent networks undergo parallel interpenetration in which the metal atoms from two networks occupy the mean plane. It is interesting to note that along a particular direction in the 2D network bpp always adopts two different conformations alternately; as a result the adjacent arms of each grid are of same conformation. Also the pyridyl rings of bpp across a metal arrange nearly perpendicular to each other (Scheme 2). The pattern of parallel interpenetration of two nets is such that crossed bpp of either grid is of opposite conformation.

In complexes **1–3** there are two independent metal centers ($M1$ = Fe1/Co1/Co1 and $M2$ = Fe2/Co2/Co2) each having slightly distorted octahedral geometry (Figs. 1–3). The amount of distortion is slightly different in the two independent metal coordination environments. Coordination bond distances and angles are given in Table 2. $M1$ is coordinated by four N atoms (N1, N2, N3 and N4) forming the equatorial plane and in this plane successive N–$M1$–N′ angles vary within 85.85(11)–95.14(11)° in **1**, 87.09(6)–94.34(6)° in **2** and 84.85(10)–98.41(12)° in **3** (Table 2). The equatorial *trans* N atoms through $M1$ deviate from linearity by 2.37° and 4.72° in **1**, 3.13° and 2.32° in **2** and 4.81° and 4.69° in **3**. The *trans* axial positions are coordinated by N (N5, N6) atoms of linear pseudohalides and slight axial distortion is reflected in the N5–$M1$–N6 angle 177.16(14)° in **1**, 178.35(6)° in **2** and 178.77(16)°, in **3**. Two pseudohalides at antipodal points align themselves at angles 25.9° and 10.1° in **1**, 20.78° and 24.60° in **2** and 14.4° and 15.0° in **3** with the axial direction (angle γ in Scheme 3).

On the other hand the N7–N10 atoms of bpp bind equatorially and N11 and N12 of two pseudohalides bind *trans* axially to the M2 metal center giving rise to slightly distorted octahedral coordination environment. Equatorial distortion is reflected in the successive N–$M2$–N′ angles (range within 87.13(14)–92.77(14)° in **1**, 87.89(6)–93.10(6)° in **2** and 83.69(11)–98.22(13)° in **3**) and the axial distortion in N11–$M2$–N12 angle (178.98(18)° in **1**, 179.73(7)° in **2** and 178.36(16)° in **3**) (Table 2). The *trans* N atoms in the equatorial plane deviate from linearity by (0.2°, 2.86°) for **1**, (2.41°, 3.01°) for **2** and (5.06°, 1.9°) for **3**. Two antipodal pseudohalides deviate from the M2 octahedron axis by (17.7°, 26.1°), (13.61°, 22.15°) and (12.5°, 18.7°) for complexes **1**, **2** and **3**, respectively. The equatorial distortion for the two metal centers is due to different conformations adopted by flexible bpp leading to a infinite 2D net. The individual nets are undulated and sinusoidal in nature and due to the parallel interpenetration of two nets a standing wave like topology for the interpenetrated layer arises.

In **1,** the Fe1 and Fe2 centers independently form 2D nets with (4,4) net topology in (110) plane with bpp adopting (TG, GG′) conformation in the Fe1 net and (TT, GG′) conformation in the Fe2 net (Fig. 4). Individual grids are rhombic with dimensions (12.83 Å × 12.25 Å) and

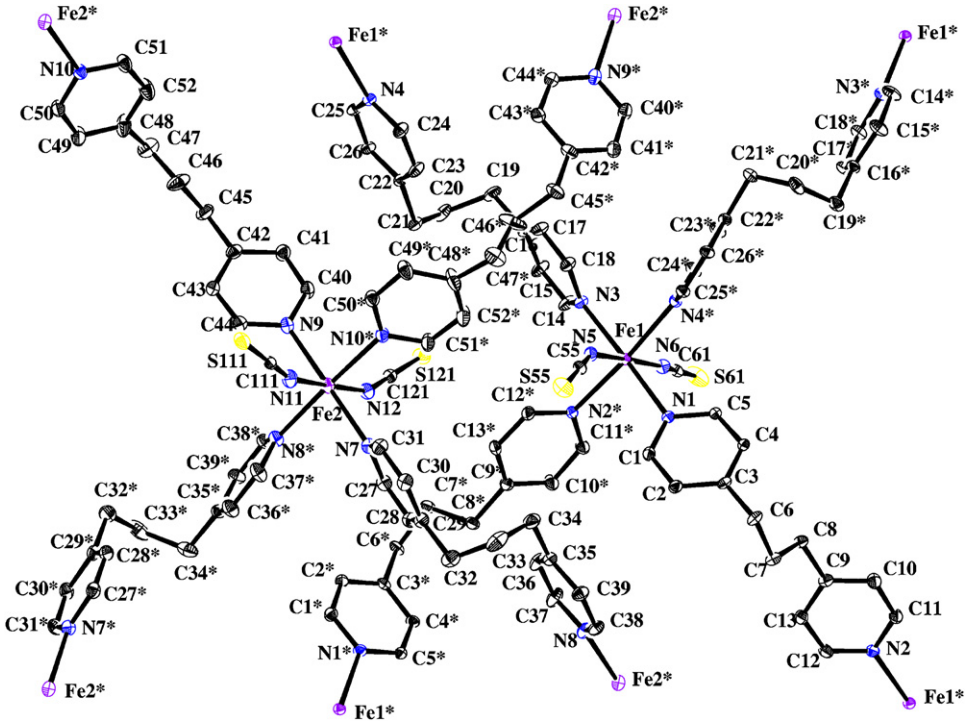

Fig. 1. ORTEP diagram of **1** having atom numbering scheme with 30% ellipsoidal probability.

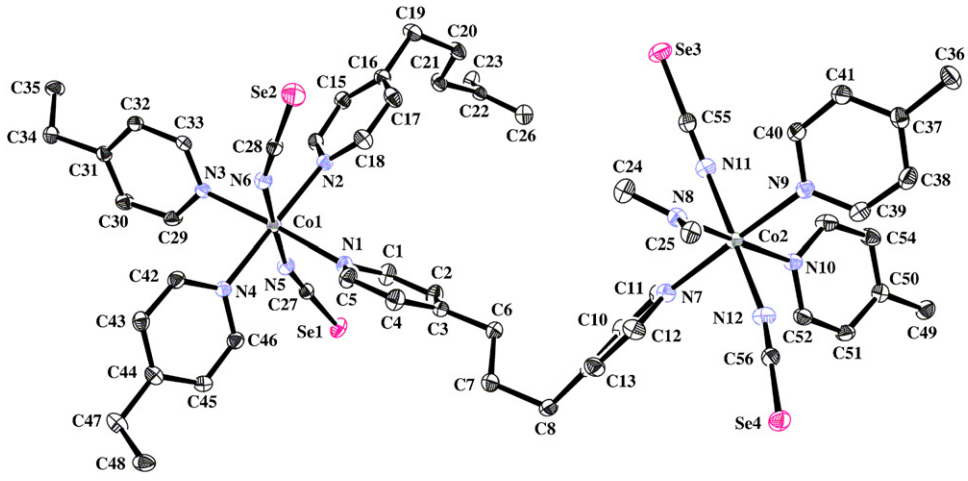

Fig. 2. ORTEP diagram of **2** having atom numbering scheme with 50% ellipsoidal probability.

(13.25 Å × 11.84 Å) for Fe1 and Fe2 net, respectively. It is to note that though bpp adopts same GG′ conformation, the N–N distance across bpp is 8.35 Å in the Fe1 net, but 8.18 Å in the Fe2 net. In TG and TT conformations these distances are 9.03 and 9.46 Å, respectively, and this trend agrees well with the one reported [33]. Recently, Proserpio et al. have classified 3D interpenetration for both metal-organic [43] and inorganic crystal structures [44] based on the symmetry relationship between the individual nets those interpenetrate. If this same concept be extended to the case of 2D interpenetration, then complex **1** is a case of non-equivalent interpenetration having the degree of interpenetration, $Z = 2(1+1)$.

In complex **2** each one of the interpenetrating nets contains both Co1 and Co2 centers and conformations of bpp in both the nets are identical (TG, GG′). It is intriguing but interesting to note that though two nearby bpp propagating the network in two perpendicular directions, have same conformation (TG or GG′) (Fig. 5), and the N–N distances of bpp are different. This suggests that even for same conformations the N⋯N distances may be different. This results different Co⋯Co separation in the nets. The N–N distance of bpp in TG conformation is 9.06 and 9.07 Å, whereas in GG′ conformation it is 8.055 and 8.47 Å. Due to this difference in same TG/GG′ conformations, smallest grid does not attain any regular geometrical

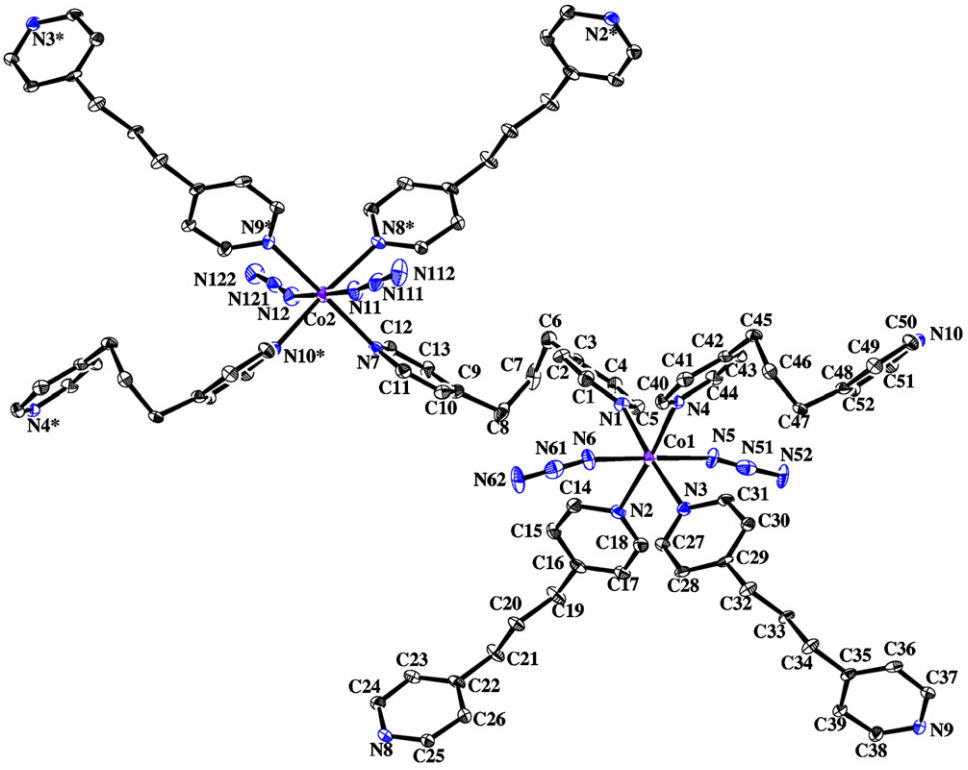

Fig. 3. ORTEP diagram of **3** having atom numbering scheme with 30% ellipsoidal probability.

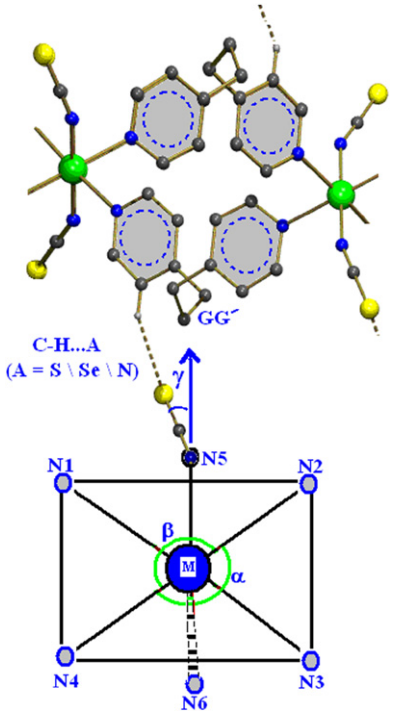

Scheme 3.

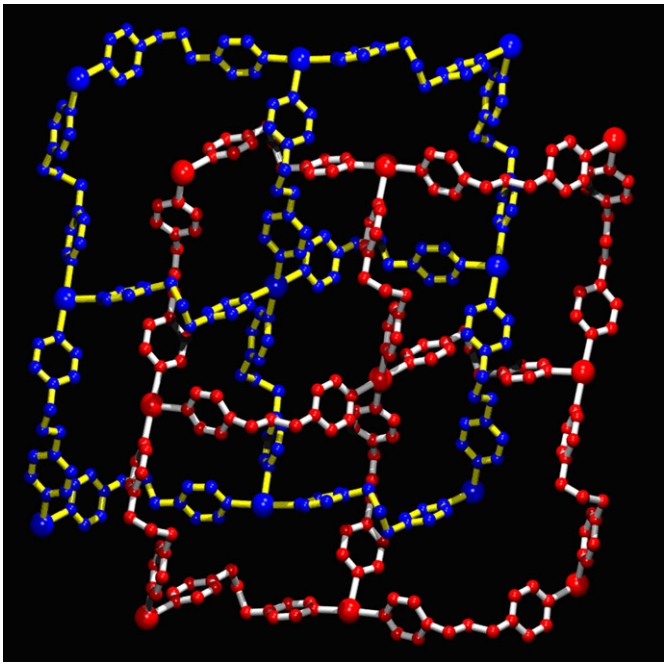

Fig. 4. 2D parallel interpenetrated network of **1** [bpp adopts (TG, GG′) conformation in net I (blue), whereas (TT, GG′) in net II (red)].

shape (in contrast to rhombic in **1**) with all unequal arms leading to smallest grid dimension (12.76 Å × 11.74 Å × 12.23 Å × 12.73 Å) (Scheme 2). Though the individual grids are not the repeating units, the union of four adjacent grids attains the rhombic shape with dimension (24.95 Å × 24.45 Å), which becomes the repeating unit. It is interesting because the symmetry at the lower level has broken but regained at higher level. Complex **2** is a case of equivalent interpenetration of Class IIa with $Z = 2$. Individual nets forming the interpenetrated layer in this case are not translationally related but are related by inversion symmetry.

Like **2** in complex **3** also there are two interpenetrating nets and individual nets contain both Co1 and Co2 centers. The smallest grid is irregular with dimension (10.88 Å × 11.18 Å × 13.69 Å × 13.79 Å). Conformations of bpp are TT and GG′, which are identical for both the nets (Fig. 6). Like **2** here also in a single net, two adjacent bpp ligands are in same conformation (TT or GG′) having different length with N–N distances, 9.63 Å; 9.72 Å for TT conformation and 7.57 Å; 7.79 Å for GG′ conformation. Complex **3** is again a case of equivalent interpenetration of Class IIa with $Z = 2$. Individual nets forming the interpenetrated layer are related by inversion symmetry.

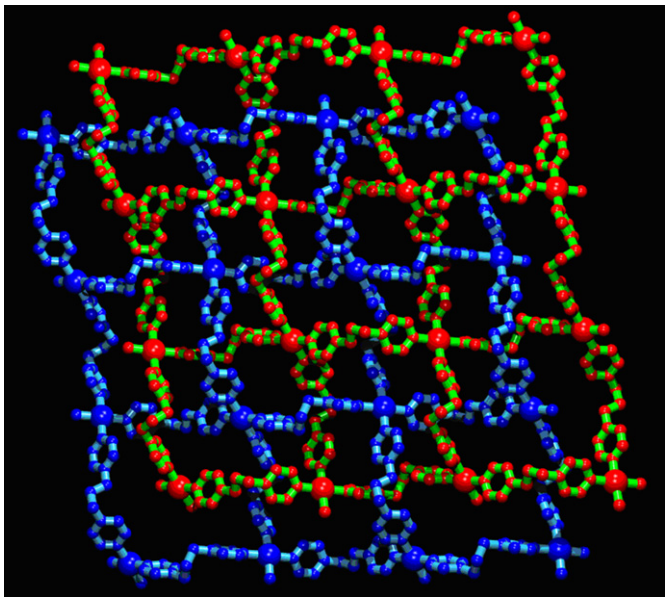

Fig. 5. 2D parallel interpenetrated network in **2** [both the nets are having (TG, GG′) conformation of bpp].

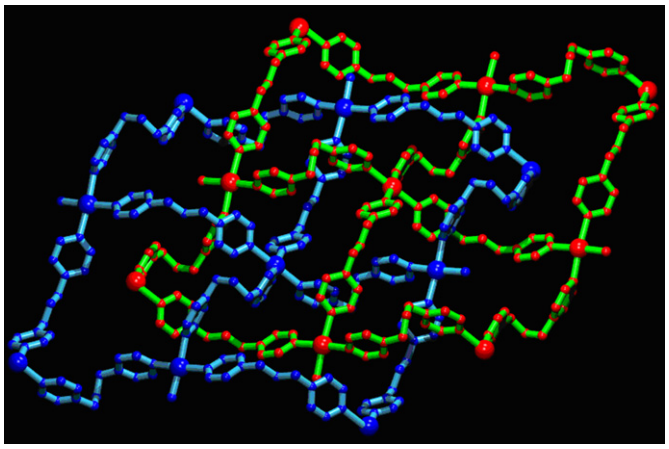

Fig. 6. 2D parallel interpenetrated network in **3** [both the nets are having (TT, GG′) conformation of bpp].

In all three complexes interpenetrated layers stack on top of the other (Figs. 7–9) with ABABA stacking sequence. The layers of two interpenetrated nets stack normal to [0,0,1] [1,−1,−1] and [1,0,1] directions, respectively, in **1, 2** and **3**. The stacking of layers has been assisted by inter layer hydrogen bonding between pendant pseudohalide of one layer and β–H of the pyridyl ring of bpp of the adjacent layer. It is interesting to note that the bpp which takes part in this inter layer hydrogen bonding always prefers GG′ conformation. In **1** the C–H···S hydrogen bond (Table 3) operates between two Fe1 bearing layers only, whereas in **2** and **3**, C–H···Se and C–H···N interactions operate between all the nets. The layers stack slightly shifted so that complementary wavy nature of both the layers match and efficient packing is achieved.

Table 4 represents the list of parallel interpenetrated 2D (4,4) nets [34–37] using bpp in combination with pseudohalide and transition metals. It shows that the conformations of bpp vary depending on the choice of pseudohalide and transition metal. bpp achieves (TG, GG′) and (TT, GG′) conformations when pseudohalide is SCN^- irrespective of transition metal (Mn/Fe/Co). It is interesting to note that in this case the two interpenetrated nets are both crystallographically independent and each of them contains only one type of metal (*M*1 or *M*2), as in case of complex **1**. According to the classification of interpenetration, these complexes are rare examples of non-equivalent interpenetrations and in case of 3D interpenetration only a limited number of this class has been found [43,45]. When the pseudohalide is N_3^-, bpp attains (TG, TG) conformation in case of Mn/Fe but (TT, GG′) in Co showing choice of metal also influences the conformation. In case of OCN^- and $SeCN^-$, bpp adopts (TT, GG′) and (TG, GG′) conformations, respectively. Some interesting observations

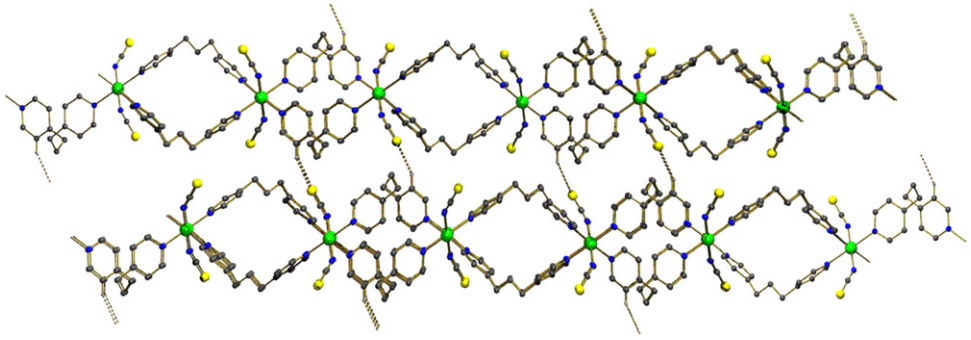

Fig. 7. Packing of successive layers through C–H···S interactions operating between net I in complex **1** (only one of the two nets in the layers has been shown for clarity).

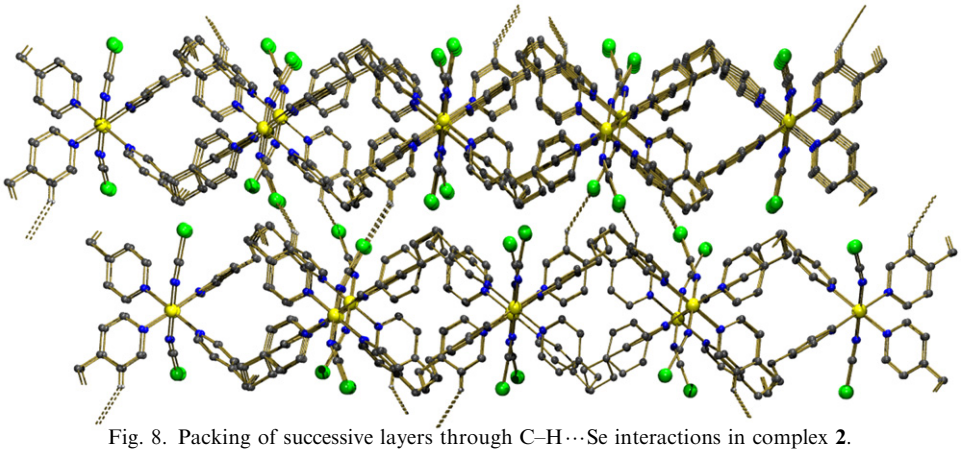

Fig. 8. Packing of successive layers through C–H···Se interactions in complex **2**.

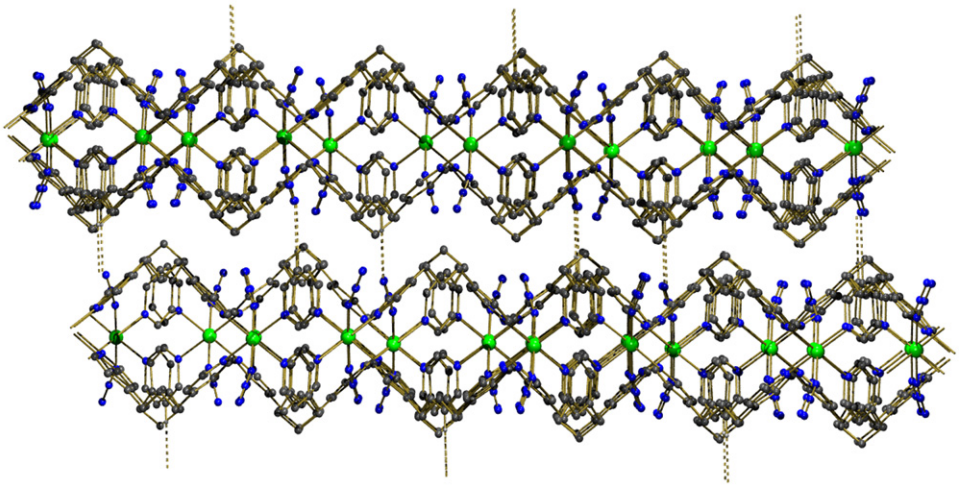

Fig. 9. Packing of successive layers through C–H···N interactions in complex **3**.

Table 4
Parallel interpenetration in complexes containing bpp ligand and pseudohalides producing 2D (4,4) nets reported so far

No.	Crystal system and space-group	Class of interpenetration[a]	Formula	Conformation of bpp and *M*–*M* distance(Å)		Ref.
				Net I	Net II	
1	Triclinic *P*-1	IIa	$[Mn_2(bpp)_4(OCN)_4]$	TT(13.825; 13.723), GG′(11.217; 10.909)	TT(13.825; 13.723), GG′(11.217; 10.909)	[35]
2	Monoclinic $P2_1/n$	Non-equivalent $Z = 2(1+1)$	$[Mn_2(bpp)_4(NCS)_4]$	TG(12.968), GG′(12.337)	TT(13.410), GG′(11.925)	[36]
3	Monoclinic $P2_1/n$	Non-equivalent $Z = 2(1+1)$	$[Fe(bpp)_2(NCS)_2]$	TG(12.825), GG′(12.254)	TT(13.258), GG′(11.848)	This work
4	Monoclinic $P2_1/n$	Non-equivalent $Z = 2(1+1)$	$[Co_2(bpp)_4(NCS)_4]$	TG(12.675), GG′(12.123)	TT(13.215), GG′ (11.625)	[37]
5	Triclinic *P*-1	IIa	$[Co_2(bpp)_4(SeCN)_4]$	TG(12.757; 12.731), GG′(12.229; 11.742)	TG(12.757; 12.731), GG′(12.229; 11.742)	This work
6	Monoclinic *C*2/*c*	Ia	$[Mn_2(bpp)_4(N_3)_4]$	TG(12.894), TG(12.894)	TG(12.894), TG(12.894)	[36]
7	Monoclinic *C*2/*c*	Ia	$[Fe_2(bpp)_4(N_3)_4]$	TG(12.782), TG(12.782)	TG(12.782), TG(12.782)	[37]
8	Triclinic *P*-1	IIa	$[Co_2(bpp)_4(N_3)_4]$	TT(13.694; 13.787),GG′ (10.885; 11.179)	TT(13.694; 13.787), GG′(10.885; 11.179)	This work

[a]For classification of interpenetration see Ref. [43].

from these complexes are, e.g., (i) there are no nets having both the conformations of bpp identical as (TT, TT) or (GG′, GG′), (ii) N_3^- in combination with Mn/Fe produces most symmetric 2D network but with Co, bpp changes conformation from the least energetic (TG, TG) to medium energetic (TT, GG′) resulting less symmetric network. The

classes of 2D interpenetration found in this type of complexes have been summarized in Table 4 which shows that the both classes Ia, IIa as well as non-equivalent interpenetration are present.

4. Conclusion

Three coordination polymers of Fe(II)/Co(II) with flexible bidentate ligand bpp and ancillary pseudohalide have been synthesized and crystallographically characterized. According to design criteria all the complexes have expected (4,4) net topology. In each case, two independent networks display parallel interpenetration due to the use of long spacer, bpp. A survey of similar complexes reveals that the conformation of bpp in complexes is different depending on the ancillary pseudohalide. There are three bpp complexes of Fe, Co and Mn with SCN^- as coligand, all having identical conformations of bpp. There is one system using OCN^-, $SeCN^-$ as coligand and three complexes using N_3^- as coligand. Fe and Mn complexes of bpp with azide have identical bpp conformation, but the Co complex shows different conformation of bpp. Though the database is too small to obtain for any statistically significant correlation regarding the influence of pseudohalide in directing the conformation of bpp, the common feature in all the complexes is that the stacking of the 2D interpenetrated layers is facilitated by the inter layer hydrogen bonding between axially bound pseudohalide and pyridyl C–H group of bpp which is in GG′ conformation. The interpenetration in the complexes is found to be of class Ia, class IIa and non-equivalent interpenetration for SCN^- bearing complexes. These observations may be useful for further exploration of coordination complexes using bpp.

Acknowledgments

Authors are thankful to Prof. K. Okamoto (University of Tsukuba) for structural data collection of one complex. A.D.J. acknowledges UGC (India) for granting leave in FIP program. G.M. acknowledges JU for a research grant of the "Nano Science and Technology Program" under the University with Potential for Excellence Scheme of UGC (India).

Appendix A. Supporting information

CCDC 645610–645612 contain the supplementary crystallographic data for **1**, **2** and **3**. These data can be obtained free of charge via http://www.ccdc.cam.ac.uk/conts/retrieving.html, or from the Cambridge Crystallographic Data Center, 12 Union Road, Cambridge CB2 1EZ, UK; fax: (+44) 1223-336-033; or e-mail: deposit@ccdc.cam.ac.uk.

References

[1] S.A. Barnett, A.J. Blake, N.R. Champness, J.E.B. Nicolson, C. Wilson, J. Chem. Soc. Dalton Trans. (2001) 567.
[2] L. Carlucci, G. Gianfranco, D.M. Proserpio, Cryst. Eng. Commun. 5 (2003) 269.
[3] Y. Diskin-Posner, G.K. Patra, I. Goldberg, Chem. Commun. (2002) 1420.
[4] K. Biradha, M. Fujita, Chem. Commun. (2002) 1866.
[5] C.-C. Wang, C.-T. Kuo, P.-T. Chou, G.-H. Lee, Angew. Chem. Int. Ed. 43 (2004) 4507.
[6] S.M.-F. Lo, S.S.-Y. Chui, L.-Y. Shek, Z. Lin, X.X. Zhang, G. Wen, I.D. Williams, J. Am. Chem. Soc. 122 (2000) 6293.
[7] S.L. James, Chem. Soc. Rev. 32 (2003) 276.
[8] Y.-Z. Zheng, M.-L. Tong, X.-M. Chen, New J. Chem. 28 (2004) 1412.
[9] H. Imai, K. Inoue, K. Kikuchi, Y. Yoshida, M. Ito, T. Sunahara, S. Onaka, Angew. Chem. Int. Ed. 43 (2004) 5617.
[10] Q. Ye, Y.-M. Song, G.-X. Wang, K. Chen, D.-W. Fu, P.W. Hong Chan, J.-S. Zhu, S.D. Huang, R.-G. Xiong, J. Am. Chem. Soc. 128 (2006) 6554.
[11] W. Zhao, J. Fan, T. Okamura, W.-Y. Sun, N. Ueyama, New J. Chem. 28 (2004) 1142.
[12] M.E. Kosal, J.-H. Chou, S.R. Wilson, K.S. Suslick, Nat. Mater. 1 (2002) 118.
[13] T.K. Maji, K. Uemura, H.-C. Chang, R. Matsuda, S. Kitagawa, Angew. Chem. Int. Ed. 43 (2004) 3269.
[14] Z. Ma, B. Moulton, Cryst. Growth Des. 7 (2007) 196.
[15] M. Casarin, C. Corvaja, C. Nicola, D. Falcomer, L. Franco, M. Monari, L. Pandolfo, C. Pettinari, F. Piccinelli, P. Tagliatesta, Inorg. Chem. 43 (2004) 5865.
[16] L. Pan, H. Liu, X. Lei, X. Huang, D.H. Olson, N.J. Turro, J. Li, Angew. Chem. Int. Ed. 42 (2003) 542.
[17] Y. Cui, O.R. Evans, H.L. Ngo, P.S. White, W. Lin, Angew. Chem. Int. Ed. 41 (2002) 1159.
[18] J.S. Seo, D. Whang, H. Lee, S.I. Jun, J. Oh, Y.J. Jeon, K. Kim, Nature 404 (2000) 982.
[19] K. Biradha, M. Fujita, Chem. Commun. (2001) 15.
[20] M.J. Plater, M.R.S.J. Foreman, T. Gelbrich, S.J. Coles, M.B. Hursthouse, J. Chem. Soc. Dalton Trans. (2000) 3065.
[21] H. Kim, M.P. Shu, Inorg. Chem. 44 (2005) 810.
[22] S.R. Batten, R. Robson, Angew. Chem. 110 (1998) 1558; S.R. Batten, R. Robson, Angew. Chem. Int. Ed. 37 (1998) 1460.
[23] S.R. Batten, Cryst. Eng. Commun. 3 (2001) 67.
[24] O.M. Yaghi, H.L. Li, C. Davis, D. Richardson, T.L. Groy, Acc. Chem. Res. 31 (1998) 474.
[25] A.J. Blake, N.R. Champness, P. Hubberstey, W.S. Li, M.A. Withersby, M. Schröder, Coord. Chem. Rev. 183 (1999) 117.
[26] S. Leininger, B. Olenyuk, P.J. Stang, Chem. Rev. 100 (2000) 853.
[27] B. Moulton, M.J. Zaworotko, Chem. Rev. 101 (2001) 1629.
[28] M. Eddaoudi, D.B. Moler, H.L. Li, B.L. Chen, T.M. Reineke, M. O'Keeffe, O.M. Yaghi, Acc. Chem. Res. 34 (2001) 319.
[29] O.R. Evans, W.B. Lin, Acc. Chem. Res. 35 (2002) 511.
[30] S.L. James, Chem. Soc. Rev. 32 (2003) 276.
[31] M. Oh, G.B. Carpenter, D.A. Sweigart, Acc. Chem. Res. 37 (2004) 1.
[32] M.J. Zaworotko, Chem. Commun. (2001) 1 and references therein.
[33] L. Carlucci, G. Ciani, D.M. Proserpio, S. Rizzato, Cryst. Eng. Commun. 4 (2002) 121.
[34] S. Konar, E. Zangrando, M.G.B. Drew, T. Mallah, J. Ribas, N. Ray Chaudhuri, Inorg. Chem. 42 (2003) 5966.
[35] A.K. Ghosh, D. Ghoshal, J. Ribas, E. Zangrando, N. Ray Chaudhuri, J. Mol. Struct. 796 (2006) 195.
[36] H. Hou, Y. Wei, Y. Song, Y. Zhu, L. Li, Y. Fan, J. Mater. Chem. 12 (2002) 838.
[37] C. Merz, M. Desciak, C. O'Brien, R.L. LaDuca, R.C. Finn, R.S. Rarig, J.A. Zubieta, Inorg. Chim. Acta 357 (2004) 3331.
[38] G.M. Sheldrick, SHELXL97, Program for Crystal Structure Refinement, University of Gottingen, Germany, 1997.
[39] G.M. Sheldrick, SHELXS 97, Program for Structure Solution, University of Gottingen, Germany, 1997.
[40] A.L. Spek, J. Appl. Crystallogr. 36 (2003) 7.

[41] L.J. Farrugia, J. Appl. Crystallogr. 30 (1997) 565.
[42] L.J. Farrugia, J. Appl. Crystallogr. 32 (1999) 837.
[43] V.A. Blatov, L. Carlucci, G. Ciani, D.M. Proserpio, Cryst. Eng. Commun. 6 (2004) 377.
[44] A. Baburin, V.A. Blatov, L. Carlucci, G. Ciani, D.M. Proserpio, J. Solid State Chem. 178 (2005) 2452.
[45] P. Metrangolo, F. Meyer, T. Pilati, D.M. Proserpio, G. Resnati, Chem. Eur. J. 13 (2007) 5765.